HHS Public Access

Author manuscript

Cell. Author manuscript; available in PMC 2017 February 25.

Published in final edited form as:

Cell. 2016 February 25; 164(5): 985–998. doi:10.1016/j.cell.2016.01.025.

Spliceosomal DEAH-box ATPases remodel pre-mRNA to activate alternative splice sites

Daniel R. Semlow[1], **Mario R. Blanco**[2,3], **Nils G. Walter**[3], and **Jonathan P. Staley**[4]

Jonathan P. Staley: jstaley@uchicago.edu

[1]Graduate Program in Cell and Molecular Biology, University of Chicago, 920 East 58th Street, Chicago, IL 60637, USA

[2]Cellular and Molecular Biology, University of Michigan, 930 North University Avenue, Ann Arbor, MI 48109, USA

[3]Department of Chemistry, Single Molecule Analysis Group, University of Michigan, 930 North University Avenue, Ann Arbor, MI 48109, USA

[4]Department of Molecular Genetics and Cell Biology, University of Chicago, 920 East 58th Street, Chicago, IL 60637, USA

Summary

During pre-mRNA splicing, a central step in the expression and regulation of eukaryotic genes, the spliceosome selects splice sites for intron excision and exon ligation. In doing so, the spliceosome must distinguish optimal from suboptimal splice sites. At the catalytic stage of splicing, suboptimal splice sites are repressed by the DEAH-box ATPases Prp16 and Prp22. Here, using budding yeast, we show that these ATPases function further by enabling the spliceosome to search for and utilize alternative branch sites and 3’ splice sites. The ATPases facilitate this search by remodeling the splicing substrate to disengage candidate splice sites. Our data support a mechanism involving 3’ to 5’ translocation of the ATPases along substrate RNA and toward a candidate site but surprisingly not across the site. Thus, our data implicate DEAH-box ATPases in acting at a distance by pulling substrate RNA from the catalytic core of the spliceosome.

Introduction

Pre-mRNA splicing is catalyzed by the spliceosome, a dynamic ribonucleoprotein (RNP) machine comprising over eighty conserved proteins and five small nuclear (sn)RNAs (Wahl et al., 2009). In the first chemical step of splicing, branching, the 2’ hydroxyl of the branch

Correspondence to: Jonathan P. Staley, jstaley@uchicago.edu.

Author Contributions

D.R.S. and J.P.S. designed experiments, interpreted data and wrote the paper with input from M.R.B. and N.G.W. D.R.S. generated reagents and performed all biochemistry experiments. D.R.S. and M.R.B. performed single molecule FRET experiments. M.R.B. performed Gaussian fitting of histograms and statistical analysis of FRET trajectories.

site adenosine (brA) attacks the 5’ splice site phosphate, cleaving the 5’ exon from the intron and forming a lariat intermediate. In the second step, exon ligation, the 3’ hydroxyl of the 5’ exon attacks the 3’ splice site phosphate, joining the exons and excising the lariat intron. Both reactions are enabled by a single catalytic core that is composed of snRNA (Fica et al., 2013; Hang et al., 2015). Within this core, U6 snRNA positions metal ions that participate directly in catalysis (Fica et al., 2013), while the U2 and U6 snRNAs form a base-pairing network that specifies and juxtaposes the reactive splice sites (Hang et al., 2015). However, it remains obscure how the spliceosome accommodates two reactions in a single catalytic core and ensures the fidelity of splice site choice.

The spliceosome faces a formidable challenge in identifying and juxtaposing the appropriate splice sites to ensure faithful gene expression (Semlow and Staley, 2012). The spliceosome must utilize optimal splice sites defined by short nucleotide motifs and discriminate against competing suboptimal splice sites, the utilization of which would corrupt the mRNA. The splice sites are first sampled during spliceosome assembly, which involves the stepwise addition of the small nuclear (sn)RNPs (Wahl et al., 2009). After the 5’ splice site is recognized by the U1 snRNP, the branch site is recognized by the U2 snRNP through base-pairing, with bulging of the nucleophilic adenosine, and then the U4/U6.U5 tri-snRNP binds. This assembly pathway and downstream steps require dramatic protein and snRNA rearrangements that depend on eight members of the SF2 superfamily of nucleic acid-dependent ATPases (Figure S1A; Wahl et al., 2009), which function ubiquitously throughout RNA-dependent processes to remodel RNP complexes (Jankowsky, 2011).

Following addition of the U4/U6.U5 tri-snRNP, the assembled but inactive spliceosome is activated in two stages. First, the SF2 ATPase Brr2 disrupts base-pairing between U6 and U4 snRNA to permit formation of interactions within U6 and between U6 and U2 snRNA, giving rise to the pre-catalytic spliceosome (Wahl et al., 2009). Then, the SF2 ATPase Prp2 promotes a more subtle rearrangement required for branching (Krishnan et al., 2013; Ohrt et al., 2012; Warkocki et al., 2015; Wlodaver and Staley, 2014). Following branching, the SF2 ATPase Prp16 and the Slu7/Prp18 heterodimer act sequentially to reposition the substrate and enable 3’ splice site recognition for exon ligation (James et al., 2002; Ohrt et al., 2013). After exon ligation, the SF2 ATPase Prp22 releases the mRNA from the spliceosome (Company et al., 1991), and the SF2 ATPase Prp43 acts with Brr2 to release the lariat intron and disassemble the spliceosome (Wahl et al., 2009).

At least five SF2 ATPases also promote the fidelity of splicing by discriminating against suboptimal splice sites (Semlow and Staley, 2012). These ATPases likely enable kinetic proofreading by competing with on-pathway events, triggering spliceosomal rearrangements that effectively “reject” suboptimal splice sites.

Despite the importance of spliceosomal SF2 ATPases, the molecular mechanisms by which these ATPase function and their consequences for splice site selection remain largely uncharacterized. Indeed, the functions and mechanisms of only a few SF2 ATPases have been defined in molecular terms (Jankowsky, 2011). Distinct SF2 families appear to perform different functions and by distinct mechanisms (Ozgur et al., 2015). The spliceosomal SF2 members belong to the DEAD-box family or the DExH-box families, which include the

Ski2-like, DEAH-box and viral NS3/NPH-II families. DEAD-box ATPases unwind duplex RNA and by directly binding and unwinding a duplex. The DExH-box families are also thought to unwind RNA but by translocating through a duplex, 3' to 5' along a single strand of RNA. Indeed, Ski2-like ATPases include a duplex melting element. However, this element is not conserved in DEAH-box or NS3/NPH-II ATPases (Jankowsky, 2011; Prabu et al., 2015), raising questions about their functions and mechanisms.

At the catalytic stage of splicing, the DEAH-box ATPases Prp16 and Prp22 also contribute to the fidelity of branching and exon ligation, respectively (Semlow and Staley, 2012). In addition to promoting repositioning of an optimal substrate after branching, Prp16 rejects suboptimal branch sites by competing with branching to remodel the spliceosome into an inactive conformation (Burgess and Guthrie, 1993; Koodathingal et al., 2010). By genetics, Prp16 appears to both reject a suboptimal substrate and promote an optimal substrate in a similar manner (Hilliker et al., 2007; Mefford and Staley, 2009; Villa and Guthrie, 2005). However, the mechanism by which Prp16 rejects a suboptimal substrate and promotes an optimal substrate remains unclear.

In addition to promoting mRNA release after exon ligation, Prp22 rejects a suboptimal 3' splice site by competing with exon ligation to remodel the spliceosome into an inactive conformation (Mayas et al., 2006). Because of these two roles, we proposed that Prp22 effects both activities by translocating upstream from the 3' exon to disrupt interactions between the spliceosome and the substrate, interactions that differ before and after exon ligation due to the changing connectivity of the substrate (Mayas et al., 2006). Indeed, mRNA release requires that Prp22 interact with the 3' exon (Schwer, 2008). However, the mechanism by which Prp22 rejects a suboptimal 3' splice site remains undefined and evidence for translocation before or after exon ligation is lacking.

The rejection of a splice site by Prp16 or Prp22 can be followed by the termination of splicing and discard of the substrate by the spliceosome-disassembly factor Prp43. However, rejection by Prp16 or Prp22 can also be followed by rebinding of the substrate (Koodathingal et al., 2010; Mayas et al., 2006), though the function of this rebinding is unknown.

Here, using budding yeast, we have investigated the function and mechanism of DEAH-box ATPases during the catalytic stage of splicing. Unexpectedly, we discovered that rejection of suboptimal splice sites by the ATPases Prp16 and Prp22 enables the spliceosome to select alternative splice sites. Utilizing single molecule fluorescence resonance energy transfer (smFRET), we found that these ATPases generally promote splice site rejection and substrate repositioning by disengaging splice sites. Finally, we revealed evidence that these ATPases reject suboptimal substrates and promote optimal substrates by translocating along substrate RNA downstream of the catalytic core but not necessarily through interactions targeted for disruption. Overall, our results support a model in which these DEAH-box ATPases function by pulling on the RNA substrate to destabilize substrate-spliceosome interactions, thereby enabling the spliceosome to sample alternative interactions with the substrate.

Results

The DEAH-box ATPase Prp16 Enables Alternative Branch Site Selection

To investigate the mechanism of Prp16-mediated branch site rejection, we designed a splicing substrate that would allow assembly of catalytically active spliceosomes but preclude branching. Specifically, we incorporated deoxyadenosine at the canonical branch site of a *UBC4* pre-mRNA, eliminating the nucleophilic 2' hydroxyl (d-brA; Figure 1A). Despite our design, in yeast whole-cell extract the d-brA substrate branched (Figure 1B, lanes 1 and 5) using an alternative branch site (see below; c.f. Query et al., 1994). Unexpectedly, depletion of Prp16, which is canonically required only for exon ligation (Figure 1B, lanes 2–4), completely abolished branching of the d-brA substrate, and wild-type, but not ATPase-defective rPrp16, rescued branching (Figure 1B, lanes 6–8). Thus, the activation of alternative branch sites required Prp16.

To test whether Prp16 was sufficient to activate alternative branch sites, we depleted Prp16 from extract, assembled spliceosomes on the d-brA substrate, and isolated the stalled spliceosomes from extract by gradient fractionation. Note that by smFRET, the pre-mRNA adopted a conformation indistinguishable from the catalytically active conformation (see below), implying that spliceosomes stalled solely due to the lack of the nucleophilic 2' hydroxyl. Importantly, wild-type, but not ATPase-defective, rPrp16 chased the isolated spliceosomes through branching; rSlu7/rPrp18 chased the spliceosomes further through exon ligation (Figure 1C). Thus, Prp16 was sufficient to activate alternative branch sites within assembled spliceosomes.

Interestingly, branching of the d-brA substrate yielded distinct lariat intermediates (Figure 1, B and C) resulting from branching at alternative adenosines 1 and 4 nucleotides (nts) upstream of the consensus branch point (Figure 1D). Because branching at −4 has not been observed in the context of canonical U2-branch site base pairing (Smith et al., 2009), branching at −4 implies that Prp16 destabilized the branch site-U2 interaction, allowing the splicing substrate to re-align with U2. Indeed, the sequence flanking this alternative branch site is complementary to U2 and bulges the nucleophilic adenosine (Figure 1D), and mutations that eliminate the complementarity precluded formation of the faster-migrating lariat intermediate (Figure S1B). Thus, we infer that in rejecting a branch site, Prp16 triggers unwinding of the U2-branchsite interaction and thereby enables the selection of alternative branch sites (see Discussion).

Prp16-mediated rejection antagonizes juxtaposition of the branch site and 5' splice site

While depletion of Prp16 stalls the d-brA substrate before branching, the spliceosome nevertheless juxtaposes the deoxyadenosine branch site with the 5' splice site (see below), suggesting that Prp16 not only disrupts the U2-branch site interaction but also antagonizes juxtaposition and reaction of the branch site with the 5' splice site. To test the possibility that Prp16 antagonizes splice site juxtaposition, we monitored splice site proximity by smFRET (Abelson et al., 2010; Blanco et al., 2015; Krishnan et al., 2013), which enables an assessment of substrate conformation in crude preparations with limiting amounts of substrate in multiple conformations. We assembled spliceosomes on *UBC4* splicing

substrates labeled with a fluorescent acceptor just upstream of the 5' splice site and a fluorescent donor just downstream of the branch site (BS-labeled; Figure 2A; Table S1; Krishnan et al., 2013). To facilitate the assignment of a FRET state to a specific intermediate, we enriched for distinct intermediates by i) stalling particular intermediates through inactivation of individual SF2 ATPases (Figure S1A), ii) isolating these intermediates from cell extract by gradient fractionation, and iii) immobilizing these intermediates on slides for total internal reflection fluorescence (TIRF) microscopy through specific affinity tags on individual spliceosomal components (Figure 2A). We then sampled emission trajectories (Figure 2A; Table S2) to generate histograms that describe the frequency with which spliceosomes at a particular intermediate stage occupy a given FRET state.

We first defined reference FRET states by assessing juxtaposition of the branch site and 5' splice site during spliceosome assembly and activation. The splicing substrate exhibited i) a zero-FRET state in assembled but catalytically inactive spliceosomes (Figure 2B), ii) a low (0.29) FRET state in pre-catalytic spliceosomes (Figure 2C), and iii) a high (0.75) FRET state in spliceosomes stalled at the branching stage (Figure 2D); FRET peaks for a specific intermediate varied with a standard deviation of ± 0.04. These FRET states were static (Figure S2A; Table S2), precluding direct analysis of substrate dynamics but still allowing assessment of substrate conformation in distinct spliceosomal subpopulations. Consistent with previous studies and thereby validating our approach (Blanco et al., 2015; Crawford et al., 2013; Krishnan et al., 2013), these increasing FRET states indicate stepwise juxtaposition of the branching reactants.

To test the consequences of Prp16-mediated rejection on the juxtaposition of the branch site with the 5' splice site, we utilized a model system for investigating proofreading *in vitro* (Figure S2B). In this system, spliceosomes stall just before branching due to U6 snRNA phosphorothioate substitutions that compromise the coordination of catalytic metals (Fica et al., 2013); this stalling is due in part to rejection by Prp16 (Koodathingal et al., 2010). Because these substitutions, unlike branch site mutations, permit efficient spliceosome assembly *in vitro*, we assayed substrate juxtaposition during Prp16-dependent rejection of one such substitution, U80-PS(S_P), in which the *pro*-S_P phosphate oxygen at nucleotide U80 is substituted with sulfur (Koodathingal et al., 2010).

As expected, isolated spliceosomes reconstituted with U6 U80-PS(S_P) and assembled on BS-labeled substrate did not catalyze branching in Mg^{2+} but did in Cd^{2+}, which restored metal binding to U80-PS(S_P) (Figure S2C). U6 U80-PS(S_P) spliceosomes that were stalled before (in Mg^{2+}) and after (in Cd^{2+}) branching both exhibited high FRET states (0.73 and 0.76, respectively; Figure 2, F and E, respectively, and H) indicating that substrate juxtaposition is not appreciably altered by branching. Spliceosomes stalled before branching by the d-brA branch site also exhibited a high FRET state (0.70; Figure S2D). These data imply that spliceosomes containing either the d-brA or U6 U80-PS(S_P) perturbation stall with the reactants poised for chemistry (Figure 1; Koodathingal et al., 2010).

We next activated Prp16-dependent rejection by incubating isolated U6 U80-PS(S_P) spliceosomes, stalled in Mg^{2+} before branching, with ATP and then immobilized

spliceosomes on slides and washed to remove ATP and unbound splicing factors, quenching the reaction. Strikingly, activation of Prp16-mediated rejection shifted U80-PS(S_P)-stalled spliceosomes from the high FRET state to a near-zero FRET state (0.07; Figure 2, G and I); this shift was blocked by the ATPase-deficient mutant rPrp16-K379A (Figure S2E). These findings further support a model in which Prp16 rejects a branch site by disrupting the U2-branchsite interaction and, as a consequence, disengaging the branch site from the 5' splice site.

Prp16 also antagonizes juxtaposition of the branch site and 5' exon after branching

To determine the consequences of Prp16 action on the juxtaposition of the 5' exon with the branch site after branching, we stalled Prp16-depleted spliceosomes just after branching, isolated these spliceosomes by gradient fractionation, added back rPrp16 and ATP (Figure S2F), and then immobilized the spliceosomes for TIRF microscopy, washing away ATP and unbound factors. Strikingly, wild-type, but not mutated, rPrp16 shifted a subpopulation of spliceosomes assembled on BS-labeled substrate from the high FRET state exhibited by the branching conformation (Figure 2J) to a near-zero FRET state indicative of an open substrate conformation (0.07; Figure 2, K and N; Figure S2G), paralleling the Prp16-dependent formation of a low FRET state before branching (compare Figure 2, F and G). Thus, after branching, Prp16 appears to function in an ATP-dependent manner to separate the products of the branching reaction, just as it appears to function before branching to separate the reactants. Because genetics have implicated unwinding of the branch site-U2 interaction after branching (Kannan et al., 2013), Prp16 may separate the branching products by disrupting this interaction, just as it does before branching (see Discussion).

To test for evidence that the Prp16-dependent, near-zero FRET state intermediate conformation is functional, we added rSlu7 and rPrp18 to the spliceosomes activated as above with rPrp16 and ATP, to drive mRNA formation (Figure S2F). Indeed, rSlu7/rPrp18 shifted a subpopulation of spliceosomes from the near-zero FRET state back to a high FRET state (0.63; Figure 2, L and O) characteristic of the exon ligation conformation (0.67; Figure 2M; Figure S1A) and with an efficiency expected given mRNA formation (Figure S2F). Note that the high FRET state at exon ligation implies that the branch site is an integral component of the catalytic core at this stage, consistent with the deleterious effects of branch site mutations at exon ligation. Overall, our data support a model in which Prp16 drives separation of the branch site and 5' exon, thereby allowing Slu7 and Prp18 to establish a proximal configuration of the branch site and 5' exon in the exon ligation conformation, a configuration that likely accommodates 3' splice site binding.

Evidence that Prp16 translocates toward but not through the branch site U2-interaction

We next investigated how Prp16 might disrupt the branch site-U2 interaction in antagonizing juxtaposition of splicing reactants before branching and products after branching. Prp16 crosslinks with substrate downstream of the branch site (McPheeters and Muhlenkamp, 2003) and unwinds model RNA duplexes with a 3' to 5' polarity (Wang et al., 1998). Thus, we hypothesized that Prp16 translocates 3' to 5' along substrate RNA, initiating downstream of the branch site and translocating toward and then across the branch site to disrupt the U2-branchsite interaction.

Consequently, to test whether Prp16-mediated rejection requires substrate downstream of the branch site, we assembled and stalled spliceosomes on the d-brA substrate in Prp16-depleted extract, isolated the spliceosomes by gradient fractionation, cleaved the spliceosome-bound substrate downstream of the branch site by oligomer-directed RNase H, and then assayed for chase through branching at alternative branch sites upon addition of ATP and rPrp16 (Figure 3A). Cleavage between +9 and +23 nucleotides, but not +16 to +33, relative to the canonical branch site blocked the Prp16-dependent chase (Figure 3A, lane 5 and 7); note that a truncation even closer to an active branch site did not compromise the branching reaction itself (Figure S3A). Thus, substrate downstream of the branch site is required for the Prp16-dependent rejection of the d-brA branch site.

We next tested whether the requirement for substrate nucleic acid downstream of the branch site was specific for RNA, because the ATPase activity of Prp16 is stimulated by ssRNA but not ssDNA (Schwer and Guthrie, 1991). The catalytic, RecA-like domains of SF2 ATPases interact with a minimum of 5 nts of RNA (Ozgur et al., 2015), so we substituted substrates with DNA in 8 nt, tiled windows downstream of the branch site (Figure 3B). With the r-brA substrate, DNA substitutions of +6 to +12 through +12 to +19 compromised branching (Figure S3B), precluding a test of whether these substitutions impede Prp16. Still, upstream DNA substitutions at +2 to +9, +3 to +10, and +4 to +11 permitted branching of the r-brA substrate (see below). In striking contrast, with the d-brA substrate the DNA substitutions at +3 to +10 and +4 to +11 inhibited branching (Figure 3C, lanes 3 and 4). Thus, the activation of alternative branch sites requires both Prp16 and RNA downstream of the branch site, supporting the model in which Prp16 interacts with the substrate downstream of the branch site and translocates upstream. Importantly, however, the DNA substitution at +2 to +9 did not inhibit branching of the d-brA substrate (Figure 3C, lane 2). Similarly, with the r-brA substrate a DNA substitution at +4 to +11 inhibited exon ligation, but the substitutions at +2 to +9 and +3 to +10 did not (Figure 3D). Thus, unexpectedly, our data suggest a refined model in which Prp16 does translocate 3’ to 5’ toward the branch site but not through the U2-branchsite interaction.

To rule out that DNA substitutions downstream of the branch site simply blocked recruitment of Prp16 to the substrate, we assayed the impact of DNA substitutions on the previously established interaction between Prp16 and substrate 18 nt downstream of the branch site (McPheeters and Muhlenkamp, 2003). We depleted Prp16 from extract, assembled spliceosomes on r-brA substrates substituted with DNA at +3 to +10 or +4 to +11 and 4-thio-U (s_4U) at +18, stalled the spliceosomes just after branching, added back rPrp16, and finally photo-activated crosslinking of the substrate with UV. With the permissive +3 to +10 DNA substitution, we observed a crosslink to Prp16 that we confirmed based on i) migration at the expected molecular weight, ii) a dependence on spliceosome activation (Figure S3, C and D), iii) a dependence on the addition of rPrp16 (Figure 3E, lanes 2 and 3), and iv) an increase with mutated rPrp16 that correlated with the accumulation of lariat intermediate (Figure 3E, lanes 3 and 4). Importantly, wild-type rPrp16 crosslinked more efficiently to the restrictive +4 to +11 DNA-substituted substrate than to the permissive +3 to +10 DNA-substituted substrate, paralleling the accumulation of the +4 to +11 lariat intermediate (Figure 3E, lane 7). Thus, the +4 to +11 DNA substitution did not block exon ligation by impeding Prp16 recruitment.

Overall, these data support the refined model in which Prp16 translocates toward but not through the U2-branch site interaction. Indeed, Prp16 also crosslinks at +11 but not at +6 (McPheeters and Muhlenkamp, 2003). Formally, Prp16 might indirectly disrupt the U2-branch site interaction by displacing a factor that interacts with the substrate downstream of the branch site, but a substitution of +2 to +9 with an equivalent-length carbon spacer, which would destabilize interactions with bound factors, permitted efficient branching (Figure 3F), and the further downstream region of +9 to +23 was accessible to RNaseH-mediated digestion (Fig. 3A), providing no evidence for functional or stable binding of factors downstream of the branch site. Further, the carbon spacer did not bypass the requirement for Prp16 (Figure 3F), arguing against a role for Prp16 in displacing a factor bound downstream of the branch site. Thus, we favor the refined model in which Prp16 translocates 3' to 5' along the substrate toward but not through the branch site. This model implies that Prp16 disrupts the U2-branch site interaction from a distance by moving the RNA substrate relative to the spliceosome, thereby pulling the substrate and applying tension sufficient to disrupt the U2-branch site interaction (see Discussion).

The DEAH-box ATPase Prp22 Enables Alternative 3' Splice Site Selection

Given the role for Prp22 in rejecting 3' splice sites (Mayas et al., 2006), we tested whether Prp22 enables the spliceosome to select alternative 3' splice sites. In the presence of extract containing only endogenous Prp22 or also exogenous wild-type rPrp22, exon ligation of a substrate with tandem alternative 3' splice sites occurred at both the upstream and downstream 3' splice sites (Figure 4A and B, lanes 1 and 2). However, in the presence of dominant negative, ATPase-defective rPrp22-K512A, which blocks rejection of a 3' splice site (Mayas et al., 2006), exon ligation occurred exclusively at the upstream 3' splice site (Figure 4B, lane 3). To test the sufficiency of Prp22 and other canonical exon ligation factors in the activation of the downstream 3' splice site, we isolated by gradient fractionation Prp16-depleted spliceosomes stalled just after branching (Figure 4C, lane 1) and then chased the spliceosomes with ATP, rPrp16, rSlu7, and rPrp18 along with wild-type or mutated rPrp22 (Figure 4C, lanes 2 and 3). Again, wild-type rPrp22 permitted splicing at both splice sites, whereas rPrp22-K512A restricted splicing to the upstream 3' splice site. Thus, use of the downstream 3' splice site requires the ATP-dependent function of Prp22, implying that recognition of the downstream 3' splice site requires Prp22-dependent rejection of the upstream 3' splice site (see Discussion), which is reminiscent of the repression of silent, upstream 3' splice sites in human splicing extract by hSlu7 (Chua and Reed, 1999), which in budding yeast recruits Prp22. We conclude that Prp22, similar to Prp16, facilitates alternative splice site selection.

Prp22-mediated rejection antagonizes juxtaposition of the 3' splice site with the 5' exon

To test whether Prp22-dependent rejection, like Prp16-dependent rejection, antagonizes juxtaposition of the reactants, we monitored splice site proximity in specific spliceosomal intermediates by smFRET using a substrate labeled with a fluorescent acceptor in the 5' exon and a fluorescent donor just downstream of the 3' splice site (3'SS-labeled substrate; Figure 5A; Table S1). This substrate efficiently reported on the juxtaposition of the 5' exon with the 3' splice site at the exon ligation stage, as revealed by a high (0.74) FRET signal (Figures 5H and S1A; Abelson et al., 2010).

We first determined the timing for juxtaposing the 3’ splice site with the 5’ exon, as above. FRET states were again static (Figure S4A and Table S2). The assembled but inactive spliceosome conformation, the pre-catalytic conformation, and the branching conformation exhibited near-zero and low FRET states (Figure 5, B to D), indicating that the 3’ splice site does not juxtapose with the 5’ splice site before or during branching. Spliceosomes stalled after branching by depletion of Prp16 and then chased with rPrp16 into the intermediate conformation remained in a low FRET state (Figures 5, E, F and I and S4B), but spliceosomes driven further into the exon ligation conformation, by the addition of rSlu7 and rPrp18, exhibited a high (0.67) FRET state (Figures 5, G and J and S4B). Thus, Prp16 first separates the 5’ exon from the branch site (Figure 2), and then Slu7 and Prp18 juxtapose the 5’ exon with the 3’ splice site, as well as the branch site (Figures 2 and 5).

We next assayed the impact of Prp22-mediated rejection on the juxtaposition of the 5’ exon with a suboptimal 3’ splice site (Figure 5P) by assembling spliceosomes on 3’SS-labeled substrate in extracts depleted of Prp16, isolating stalled spliceosomes by gradient fractionation (Figure 5, K and Q), and then chasing with rPrp16, rSlu7, and rPrp18 and either wild-type or ATPase-defective rPrp22 (Figure 5, L, M, R, and S and Figure S4C). For both an optimal and a suboptimal 3’ splice site, spliceosomes treated with rPrp22-K512A exhibited high FRET states indicating juxtaposition of the 5’ exon and 3’ splice site in the exon ligation conformation (Figure 5, K, L, N, Q, R, and T); the suboptimal 3’ splice site, like an optimal site (Figure 2M), also permitted juxtaposition of the 5’ exon and branch site in the exon ligation conformation (Figure S4, D to F). For the optimal 3’ splice site substrate, wild-type rPrp22, relative to mutant, only slightly decreased the frequency of the high FRET state (Figure 5, M and O). Importantly, for the suboptimal 3’ splice site, wild-type Prp22, relative to mutant, shifted a significant fraction of spliceosomes to a zero-FRET state (Figure 5, S and U). Thus, Prp22-dependent rejection before exon ligation promotes separation of potential reactants, just as Prp16 does before branching.

Evidence that Prp22 translocates toward but not through its target

Previously, we proposed that Prp22, as a 3’ to 5’ DEAH-box ATPase (Tanaka and Schwer, 2005), rejects a 3’ splice site or releases mRNA by translocating from the 3’ exon upstream to disrupt interactions between the substrate and the spliceosome (Mayas et al., 2006; see Introduction). Indeed, Prp22-dependent mRNA release requires at least 13 nts in the 3’ exon (Schwer, 2008). Thus, we tested whether truncation of a 3’ exon inhibited Prp22-dependent rejection of a 3’ splice site that competes with a second, downstream 3’ splice site (Figure 4). With a control substrate lacking the upstream 3’ splice site, truncation of the 3’ exon to 3 nt in length did not impact the efficiency of exon ligation at the downstream 3’ splice site (Figure 6A, lanes 1 and 2). However, in contrast to the full-length, tandem 3’ splice site substrate, which spliced at both 3’ splice sites (Figure 4B; Figure 6A, lane 3), a truncated, tandem 3’ splice site substrate spliced only at the upstream 3’ splice site (Figure 6A, lane 4). Thus, recognition of the downstream 3’ splice site, when in competition with the upstream 3’ splice site, required both Prp22 and substrate downstream, implying that Prp22 promotes 3’ splice site rejection, like mRNA release, by translocating from the 3’ exon in a 3’ to 5’ direction.

To test for evidence that Prp22, like Prp16, translocates toward but not through its target, we again substituted segments of the substrate with DNA, because the ATPase activity of Prp22 is similarly stimulated by ssRNA but not ssDNA and Prp22 cannot unwind a substrate with 3’ ssDNA tail (Schwer, 2008; Tanaka and Schwer, 2005). Because substitutions in the intron and 3’ exon compromise Prp2 and Prp16 function, we could not investigate the impact of DNA substitutions on Prp22-mediated rejection of a 3’ splice site. Instead, we investigated the impact of DNA substitutions on Prp22-mediated release of mRNA using substrates substituted with DNA at regions flanking the exon-exon junction or within the 5’ exon (Figure 6B). By gradient fractionation of splicing reactions, unsubstituted mRNA released efficiently (71%), but mRNA substituted with DNA from −4 to +4 and from −8 to −1, relative to the exon-exon junction, did not (14% and 9%, respectively; Figure 6C). However, mRNAs substituted with DNA in the window of −9 to −2 did release efficiently (66%; Figure 6C) and in a Prp22-dependent manner (Figure S5A). Because the spliceosome footprints at least 13 nt of the 5’ exon (Figure S5B; Schwer, 2008), these data do not support a model in which Prp22 must translocate through the mRNA-spliceosome interaction, although the data do suggest a requirement to translocate partially into the interaction.

To rule out that DNA substitutions impaired mRNA release by simply blocking recruitment rather than translocation of Prp22, we assayed for the impact of DNA substitution on the interaction between Prp22 and the 3’ exon established previously by s_4U crosslinking (Schwer, 2008). We supplemented Prp22-depleted extract with rPrp22-K512A, assembled spliceosomes on substrate substituted with s_4U at +17 relative to the exon-exon junction, and then induced crosslinking with UV (Figure 6D). With the all-RNA substrate, we observed a crosslink to Prp22 that we confirmed based on i) migration at the expected molecular weight, ii) a dependence on substrate repositioning by Prp16 (Figure S5C), and iii) dependence on the presence of rPrp22-K512A (Figure 6D, lanes 2 with 4). Importantly, with the restrictive −4 to +4 DNA-substituted substrate, mutated rPrp22 crosslinked just as efficiently, in correlation with the extent of mRNA formed (Figure 6D, compare lanes 2 with 4 and 6 with 8). These data indicate that the −4 to +4 DNA substitution that blocked mRNA release did not block the interaction between Prp22 and the 3’ exon, implying that the DNA substitution instead blocked translocation of Prp22p upstream toward the exon-exon junction. Overall, our data are consistent with a model in which Prp22 translocates along the 3’ exon, moving the mRNA relative to the spliceosome to apply tension sufficient to disrupt substrate-spliceosome interactions.

Discussion

During splicing, the spliceosome ensures specificity in selecting splice sites, but the mechanisms that facilitate splice site selection beyond spliceosome assembly have not been well understood. In this work, we establish that the DEAH-box ATPases Prp16 and Prp22 contribute to splice site selection at the catalytic stage (Figures 1 and 4). We also provide evidence that these ATPases antagonize the juxtaposition of splice sites, thereby rejecting suboptimal splice sites before they react and enabling substrate repositioning for exon ligation after branching of optimal splice sites (Figures 2 and 5). Finally, we present evidence that these ATPases function through a mechanism involving translocation 3’ to 5’ along substrate RNA toward but not through their targets (Figures 3 and 6), suggesting that

they disrupt interactions between the substrate and the spliceosome by limited translocation that manifests as pulling of the substrate out of the catalytic core. Together, our data identify Prp16 and Prp22 as RNP chaperones that allow the spliceosome to search for splice sites (Figure 7A).

Just as a subset of RNA chaperones destabilize non-native ribozyme conformations to allow formation of an open conformation that then enables sampling of alternative conformations (Herschlag, 1995), Prp16 and Prp22 destabilize interactions between suboptimal splice sites and the spliceosome to promote formation of an open conformation (Figures 2, 5, and 7A), from which the spliceosome can sample alternative splice sites toward ultimately identifying an optimal splice site (Figure 7A). Indeed, our evidence that Prp16 disrupts the U2-branch site interaction rationalizes the Prp16-dependent proofreading of non-consensus branch sites (Burgess and Guthrie, 1993) that would bind U2 more weakly and unwind more readily. Additionally, like RNA chaperones, these DEAH-box ATPases enable escape from kinetic traps. For example, spliceosomes stalled on the d-brA substrate are stable for hours – until Prp16 acts (Figure 1). Further, just after branching, the spliceosome is kinetically trapped, unable to transition through an intermediate conformation to the exon ligation conformation (Ohrt et al., 2013) – until Prp16 acts. Our data indicate that Prp16 overcomes this kinetic trap by separating the 5’ splice site and branch site (Figure 2K), yielding an open conformation that then enables the spliceosome to sample the substrate for a 3’ splice site for exon ligation (Figure 2, Figure 5, and Figure 7A).

By demonstrating that Prp16-dependent rejection of a suboptimal branch site permits usage of alternative branch sites (Figure 1 and Figure 7A), we provide insight into the recognition and rearrangement of the branch site during splicing. Although the U2-branch site helix can accommodate bulging of the nucleophile at multiple positions (Query et al., 1994; Smith et al., 2009), our data indicate that Prp16-dependent destabilization of the U2-branch site interaction is required for sampling of these alternative bulges (Figure 1D). We therefore conclude that U2 binds the branch site with the canonical adenosine bulged and fixes this register throughout assembly and catalytic activation of the spliceosome. Because alternative positions are selected as the nucleophile only after Prp16-dependent rejection, branch site selection must be less constrained after Prp16-dependent rejection than during assembly, though complementarity with U2 remains a requirement (Figure S1B). Importantly, genetic data have implicated parallel roles for Prp16 before and after branching and disruption of the U2-branch site helix before and after branching (Kannan et al., 2013; Semlow and Staley, 2012; Smith et al., 2007). The parallel between Prp16-dependent separation of the 5’ splice site and branch site before branching and of the 5’ exon and branch site afterwards (Figure 2) supports a role for Prp16 in disrupting the U2-branch site interaction after branching, which provides a mechanism for branch site repositioning within the catalytic core to accommodate juxtaposition of the 5’ exon and 3’ splice site for exon ligation.

In addition to disrupting the U2-branch site interaction, Prp16 also promotes toggling of snRNA structures. Genetics have implicated Prp16 in the destabilization of U2/U6 helix Ia, which juxtaposes the 5’ splice site and branch site (Mefford and Staley, 2009). Indeed, Prp16 drove spliceosomes assembled on the BS-labeled substrate into a low FRET state nearly as low as the FRET state occupied by spliceosomes stalled before U4/U6 unwinding and

U2/U6 helix Ia formation (Figure 2, compare B and G). Disruption of this helix by Prp16 would facilitate separation of the 5' splice site and a suboptimal branch site before branching and may result indirectly from disruption of the adjacent U2-branch site interaction. Genetics have also suggested that Prp16 promotes toggling of U2 from one conformation, stem IIc, to a mutually exclusive conformation, stem IIa (Hilliker et al., 2007; Perriman and Ares, 2007). Given that U2 stem IIa is adjacent to the branch site binding region of U2, toggling to the stem IIa conformation may reposition the branch site binding region of U2 away from the branch site and facilitate sampling of alternative branch sites.

Our data suggest a model for Prp16-dependent remodeling of the U2-branch site interaction in which Prp16 disrupts the interaction from a distance (Figures 3, 7B). In this model, Prp16 translocates along the substrate 3' to 5' from downstream of the catalytic core, but because Prp16 would remain anchored to the spliceosome, Prp16 would function as a molecular winch, moving the RNA substrate relative to the spliceosome, applying tension to the U2-branch site interaction and ultimately pulling the branch site off of U2. Importantly, this model provides a mechanism for unwinding a duplex that would otherwise be inaccessible to SF2 ATPases, such as DEAD-box ATPases (Ozgur et al., 2015), that require direct interaction with a duplex target.

Translocation along the substrate toward, but not necessarily through, interactions targeted for disruption, appears to be a general mechanism for DEAH-box ATPases at the catalytic stage of splicing. Prp22-dependent rejection of a 3' splice site and mRNA release also requires substrate downstream of the catalytic core (Figure 6A; Schwer, 2008), consistent with a model in which Prp22 translocates from the 3' exon upstream to disrupt interactions between the substrate and the spliceosome (Mayas et al., 2006). Further, our data indicate that Prp22-dependent mRNA release requires RNA upstream from its initial site of interaction with the 3' exon but only up to the last nucleotide of the 5' exon (Figure 6C and D). Thus, Prp22 can displace the spliceosome from mRNA without translocating entirely through interactions between the spliceosome and mRNA, interactions that extend ~15 nts upstream of the exon-exon junction. Prp22 and Prp16 may therefore share a common mechanism that involves loading onto substrate RNA downstream of the catalytic core and translocating to move the RNA substrate relative to the spliceosome, thereby pulling the substrate out of the catalytic core (Figure 7B). Consistent with a common mechanism, excess rPrp22 can partially substitute for Prp16 in chasing Prp16-depleted spliceosomes through exon ligation (Figure S6).

The mechanistic link between Prp22-dependent rejection of a 3' splice site and recognition of an alternative 3' splice site (Figure 4 and Figure 6A) provides a basis for reconciling divergent views on the mechanism of 3' splice site selection (Perez-Valle and Vilardell, 2012). The exclusive selection of an upstream 3' splice site over a downstream 3' splice site in a bimolecular splicing assay has provided strong support for the proposal that the spliceosome employs a linear 5' to 3' scanning mechanism to identify the nearest 3' splice site downstream of the branch site (Chen et al., 2000). Nevertheless, a 3' splice site, if close to the branch site, lacking a strong polypyrimidine tract, or deviating from the consensus, can be skipped in favor of a downstream 3' splice site, leading to the confounding conclusion that scanning can be "leaky" (Patterson and Guthrie, 1991; Smith et al., 1993) or

that 3’ splice site selection is instead controlled by a diffusion-collision model (Umen and Guthrie, 1995). Our data indicate that Prp22 is required specifically for recognition of a downstream 3’ splice site (Figure 4) and can therefore account for the leaky feature of the scanning model and thereby support this model. We propose that the spliceosome scans to the first upstream 3’ splice site but that Prp22-dependent rejection can allow the spliceosome to dissociate the 3’ splice site and scan further downstream (Figure 4B). In our model, sequence determinants that disfavor an upstream site would sensitize the upstream 3’ splice site to Prp22-dependent rejection and facilitate scanning for downstream 3’ splice sites, a mechanism that could be targeted for regulation. Indeed, given that such DEAH-box ATPases are essential components of the splicing pathway, these factors are well positioned to control a wide variety of alternative splicing events. Further, given the breadth of this family of ATPases, they are similarly well positioned to control substrate specificity in a broad array of RNA-dependent processes.

Experimental Procedures

See Extended Experimental Procedures and Table S1 for details.

In Vitro Splicing and Isolation of Spliceosomal Intermediates

Splicing reactions containing 0.4 nM ^{32}P-labeled or 4 nM fluorescently-labeled substrate (Abelson et al., 2010; Krishnan et al., 2013) were incubated at 20 °C for 30–60 min under standard splicing conditions with 2 mM ATP and yeast whole-cell extract (Mayas et al., 2006) and inspected by denaturing PAGE. To stall spliceosomal intermediates for TIRF microscopy, yeast whole-cell extract was either immunodepleted of Prp16; supplemented with exogenous rPrp2-K252A, rPrp16-K379A, or rPrp22-K512A; or depleted of U6 and reconstituted with synthetic U6 containing the U80-PS(*SP*) atomic substitution (Fica et al., 2013); assembled, but catalytically-inactive, spliceosomes were stalled with a low ATP concentration of 0.1 mM (Tarn el al., 1993). Splicing reactions were separated on 15–40% glycerol gradients and fractions containing spliceosomal intermediates were collected and stored at −80 °C. Isolated spliceosomal intermediates were either directly immobilized for TIRF microscopy or first chased under standard splicing conditions with ATP, divalent metal, and/or exogenous splicing factors.

TIRF Microscopy

Stalled or chased spliceosomes were immobilized via biotinylated Prp19p or Prp8p that bound to streptavidin on the surface of PEG-passivated quartz slides. Immobilized spliceosomes were washed to remove ATP and exogenous splicing factors and then imaged in splicing buffer lacking ATP. Single molecule donor and acceptor emission trajectories were collected using a prism-based TIRF microscope with direct excitation of the donor fluorophore (Abelson et al., 2010). Presence of the acceptor fluorophore was confirmed by direct excitation. Individual donor and acceptor trajectories were filtered by visual inspection (Blanco and Walter, 2010) and then FRET values were calculated. Histograms describing the distribution of FRET values for a given population of spliceosomes were constructed by sampling the first 10 frames of data (1 s total) for each spliceosome. All

reported changes in FRET distribution were observed in at least two independent spliceosome preparations.

Mapping the Branch Sites of Lariat Intermediates Formed by the br-dA Substrate

To map branch sites, 5'-^{32}P-labeled DNA primer (Table S1) was annealed to lariat intermediates and extended using AMV reverse transcriptase (Promega) according to the manufacturer's instructions. Primer extension stops were inspected by denaturing PAGE.

UV Crosslinking

Splicing substrates were site specifically modified with s_4U and an associated ^{32}P radiolabel. Splicing reactions were irradiated with 365 nm UV and digested with RNase T1 before analysis.

mRNA Release Assays

Splicing reactions were incubated at 20 °C for 60 min and then separated on 15–40% glycerol gradients. Fractions were collected from the tops of gradients, and inspected by denaturing PAGE.

Supplementary Material

Refer to Web version on PubMed Central for supplementary material.

Acknowledgments

We thank B. Schwer and C. Guthrie for plasmids and antibodies; J. Abelson and C. Guthrie for sharing unpublished data; members of the Staley and Walter laboratories for helpful discussions, especially S. Fica, M. Kahlscheuer, and R. Toroney who also provided experimental assistance; and C. Guthrie, A. Hoskins and J. Piccirilli for comments on the manuscript. D.R.S. and M.R.B. were supported by the Genetics and Regulation Training Grant (T32GM07197) and the Cellular and Molecular Biology Training Grant (T32GM007315), respectively, both from the National Institutes of Health (NIH). This work was funded by grants to J.P.S. (R01GM062264 and R01GM062264-08S1) and N.G.W (R01GM098023) from the NIH.

References

Abelson J, Blanco M, Ditzler MA, Fuller F, Aravamudhan P, Wood M, Villa T, Ryan DE, Pleiss JA, Maeder C, et al. Conformational dynamics of single pre-mRNA molecules during *in vitro* splicing. Nat. Sruct. Mol. Bology. 2010; 17:504–512.

Blanco M, Walter NG. Analysis of complex single-molecule FRET time trajectories. Methods Enzymol. 2010; 472:153–178. [PubMed: 20580964]

Blanco MR, Martin JS, Kahlscheuer ML, Krishnan R, Abelson J, Laederach A, Walter NG. Single molecule cluster analysis dissects splicing pathway conformational dynamics. Nat. Methods. 2015; 12:1077–1084. [PubMed: 26414013]

Burgess SM, Guthrie C. A mechanism to enhance mRNA splicing fidelity: the RNA-dependent ATPase Prp16 governs usage of a discard pathway for aberrant lariat intermediates. Cell. 1993; 73:1377–1391. [PubMed: 8324826]

Chen S, Anderson K, Moore MJ. Evidence for a linear search in bimolecular 3' splice site AG selection. Proc. Natl. Acad. Sci. U.S.A. 2000; 97:593–598. [PubMed: 10639124]

Chua K, Reed R. The RNA splicing factor hSlu7 is required for correct 3' splice-site choice. Nature. 1999; 402:207–210. [PubMed: 10647016]

Company M, Arenas J, Abelson J. Requirement of the RNA helicase-like protein Prp22 for release of messenger RNA from spliceosomes. Nature. 1991; 349:487–493. [PubMed: 1992352]

Crawford DJ, Hoskins AA, Friedman LJ, Gelles J, Moore MJ. Single-molecule colocalization FRET evidence that spliceosome activation precedes stable approach of 5' splice site and branch site. Proc. Natl. Acad. Sci. U.S.A. 2013; 110:6783–6788. [PubMed: 23569281]

Fica SM, Tuttle N, Novak T, Li NS, Lu J, Koodathingal P, Dai Q, Staley JP, Piccirilli JA. RNA catalyses nuclear pre-mRNA splicing. Nature. 2013; 503:229–234. [PubMed: 24196718]

Hang J, Wan R, Yan C, Shi Y. Structural basis of pre-mRNA splicing. Science. 2015; 349:1191–1198. [PubMed: 26292705]

Herschlag D. RNA chaperones and the RNA folding problem. J. Biol. Chem. 1995; 270:20871–20874. [PubMed: 7545662]

Hilliker AK, Mefford MA, Staley JP. U2 toggles iteratively between the stem IIa and stem IIc conformations to promote pre-mRNA splicing. Genes Dev. 2007; 21:821–834. [PubMed: 17403782]

James SA, Turner W, Schwer B. How Slu7 and Prp18 cooperate in the second step of yeast pre-mRNA splicing. RNA. 2002; 8:1068–1077. [PubMed: 12212850]

Jankowsky E. RNA helicases at work: binding and rearranging. Trends Biochem. Sci. 2011; 36:19–29. [PubMed: 20813532]

Kannan R, Hartnett S, Voelker RB, Berglund JA, Staley JP, Baumann P. Intronic sequence elements impede exon ligation and trigger a discard pathway that yields functional telomerase RNA in fission yeast. Genes Dev. 2013; 27:627–638. [PubMed: 23468430]

Koodathingal P, Novak T, Piccirilli JA, Staley JP. The DEAH box ATPases Prp16 and Prp43 cooperate to proofread 5' splice site cleavage during pre-mRNA splicing. Mol. Cell. 2010; 39:385–395. [PubMed: 20705241]

Krishnan R, Blanco MR, Kahlscheuer ML, Abelson J, Guthrie C, Walter NG. Biased Brownian ratcheting leads to pre-mRNA remodeling and capture prior to first-step splicing. Nat. Struct. Mol. Biol. 2013; 20:1450–1457. [PubMed: 24240612]

Mayas RM, Maita H, Semlow DR, Staley JP. Spliceosome discards intermediates via the DEAH box ATPase Prp43p. Proc. Natl. Acad. Sci. U.S.A. 2010; 107:10020–10025. [PubMed: 20463285]

Mayas RM, Maita H, Staley JP. Exon ligation is proofread by the DExD/H-box ATPase Prp22p. Nat. Struct. Mol. Biol. 2006; 13:482–490. [PubMed: 16680161]

McPheeters DS, Muhlenkamp P. Spatial organization of protein-RNA interactions in the branch site-3' splice site region during pre-mRNA splicing in yeast. Mol. Cell. Bio.l. 2003; 23:4174–4186.

Mefford MA, Staley JP. Evidence that U2/U6 helix I promotes both catalytic steps of pre-mRNA splicing and rearranges in between these steps. RNA. 2009; 15:1386–1397. [PubMed: 19458033]

Ohrt T, Odenwälder P, Dannenberg J, Prior M, Warkocki Z, Schmitzová J, Karaduman R, Gregor I, Enderlein J, Fabrizio P, et al. Molecular dissection of step 2 catalysis of yeast pre-mRNA splicing investigated in a purified system. RNA. 2013; 19:902–915. [PubMed: 23685439]

Ohrt T, Prior M, Dannenberg J, Odenwalder P, Dybkov O, Rasche N, Schmitzová J, Gregor I, Fabrizio P, Enderlein J, et al. Prp2-mediated protein rearrangements at the catalytic core of the spliceosome as revealed by dcFCCS. RNA. 2012; 18:1244–1256. [PubMed: 22535589]

Ozgur S, Buchwald G, Falk S, Chakrabarti S, Prabu JR, Conti E. The conformational plasticity of eukaryotic RNA-dependent ATPases. FEBS. J. 2015; 282:850–863. [PubMed: 25645110]

Patterson B, Guthrie C. A U-rich tract enhances usage of an alternative 3' splice site in yeast. Cell. 1991; 64:181–187. [PubMed: 1846089]

Perez-Valle J, Vilardell J. Intronic features that determine the selection of the 3' splice site. Wiley Interdiscip. Rev. RNA. 2012; 3:707–717. [PubMed: 22807288]

Perriman RJ, Ares M Jr. Rearrangement of competing U2 RNA helices within the spliceosome promotes multiple steps in splicing. Genes Dev. 2007; 21:811–820. [PubMed: 17403781]

Prabu JR, Müller M, Thomae AW, Schüssler S, Bonneau F, Becker PB, Conti E. Structure of the RNA helicase MLE reveals molecular mechanisms for uridine specificity and RNA-ATP coupling. Mol. Cell. 2015; 6:487–499. [PubMed: 26545078]

Query CC, Moore MJ, Sharp PA. Branch nucleophile selection in pre-mRNA splicing: evidence for the bulged duplex model. Genes Dev. 1994; 8:587–597. [PubMed: 7926752]

Schwer B. A conformational rearrangement in the spliceosome sets the stage for Prp22-dependent mRNA release. Mol. Cell. 2008; 30:743–754. [PubMed: 18570877]

Schwer B, Guthrie C. Prp16 is an RNA-dependent ATPase that interacts transiently with the spliceosome. Nature. 1991; 349:494–499. [PubMed: 1825134]

Schwer B, Guthrie C. A conformational rearrangement in the spliceosome is dependent on Prp16 and ATP hydrolysis. EMBO. J. 1992; 11:5033–5039. [PubMed: 1464325]

Semlow DR, Staley JP. Staying on message: ensuring fidelity in pre-mRNA splicing. Trends Biochem. Sci. 2012; 37:263–273. [PubMed: 22564363]

Smith CW, Chu TT, Nadal-Ginard B. Scanning and competition between AGs are involved in 3' splice site selection in mammalian introns. Mol. Cell. Biol. 1993; 13:4939–4952. [PubMed: 8336728]

Smith DJ, Konarska MM, Query CC. Insights into branch nucleophile positioning and activation from an orthogonal pre-mRNA splicing system in yeast. Mol. Cell. 2009; 34:333–343. [PubMed: 19450531]

Smith DJ, Query CC, Konarska MM. trans-splicing to spliceosomal U2 snRNA suggests disruption of branch site-U2 pairing during pre-mRNA splicing. Mol. Cell. 2007; 26:883–890. [PubMed: 17588521]

Tanaka N, Schwer B. Characterization of the NTPase, RNA-binding, and RNA-helicase activities of the DEAH-box splicing factor Prp22. Biochemistry. 2005; 44:9795–9803. [PubMed: 16008364]

Tarn W-Y, Lee K-R, Cheng S-C. Yeast precursor mRNA processing protein PRP19 associates with the spliceosome concomitant with or just after dissociation of U4 small nuclear RNA. Proc. Natl. Acad. Sci. U.S.A. 1993; 90:10821–10825. [PubMed: 8248176]

Umen JG, Guthrie C. The second catalytic step of pre-mRNA splicing. RNA. 1995; 1:869–885. [PubMed: 8548652]

Villa T, Guthrie C. The Isy1p component of the NineTeen complex interacts with the ATPase Prp16p to regulate the fidelity of pre-mRNA splicing. Genes Dev. 2005; 19:1894–1904. [PubMed: 16103217]

Wahl MC, Will CL, Lührmann R. The spliceosome: design principles of a dynamic RNP machine. Cell. 2009; 136:701–718. [PubMed: 19239890]

Wang Y, Wagner JD, Guthrie C. The DEAH-box splicing factor Prp16 unwinds RNA duplexes *in vitro*. Curr. Biol. 1998; 8:441–451. [PubMed: 9550699]

Warkocki Z, Schneider C, Mozaffari-Jovin S, Schmitzová J, Höbartner C, Fabrizio P, Lührmann R. The G-patch protein Spp2 couples the spliceosome-stimulated ATPase activity of the DEAH-box protein Prp2 to catalytic activation of the spliceosome. Genes Dev. 2015; 29:94–107. [PubMed: 25561498]

Wlodaver AM, Staley JP. The DExD/H-box ATPase Prp2p destabilizes and proofreads the catalytic RNA core of the spliceosome. RNA. 2014; 20:282–294. [PubMed: 24442613]

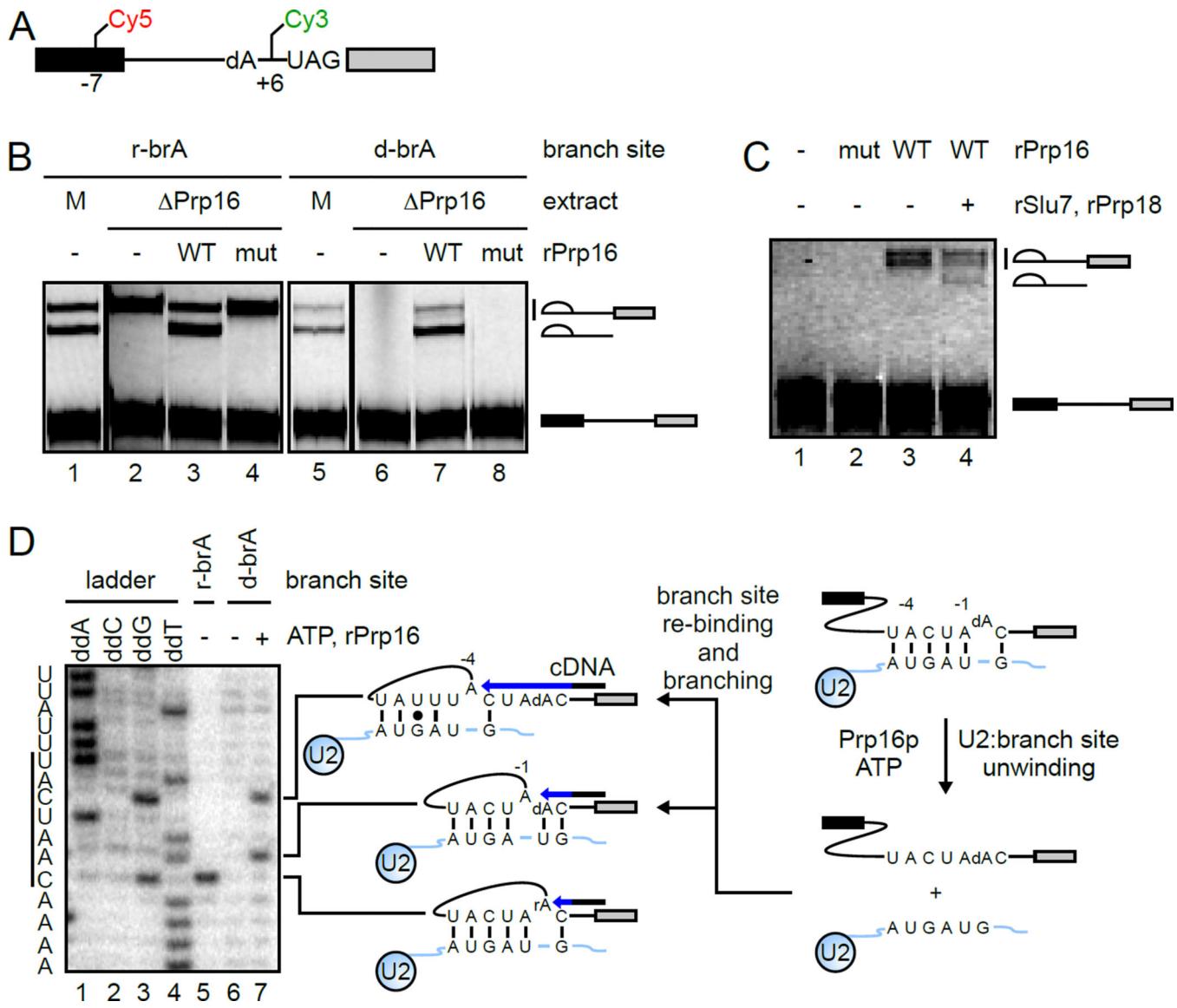

Figure 1. Prp16 Promotes Sampling of Alternative Branch Sites

(**A**) Schematic of synthetic fluorescently-labeled splicing substrate with a deoxyadenosine substitution at the canonical branch site (d-brA). (**B**) Splicing of r-brA and d-brA substrates was tested in mock-(M) or Prp16-depleted (ΔPrp16) extract supplemented with exogenous wild-type (WT) or K379A mutated (mut) rPrp16. (**C**) Isolated, Prp16-depleted spliceosomes assembled on d-brA substrate were incubated with the indicated factors. Splicing was visualized in (B) and (C) via Cy3. (**D**) The r-brA and d-brA substrate branch points were mapped by extension of a P^{32}-labeled primer. Stops occur 1 nt downstream of the branch site, as diagrammed. The inferred activity of Prp16 is modeled in the cartoon. See also Figure S1.

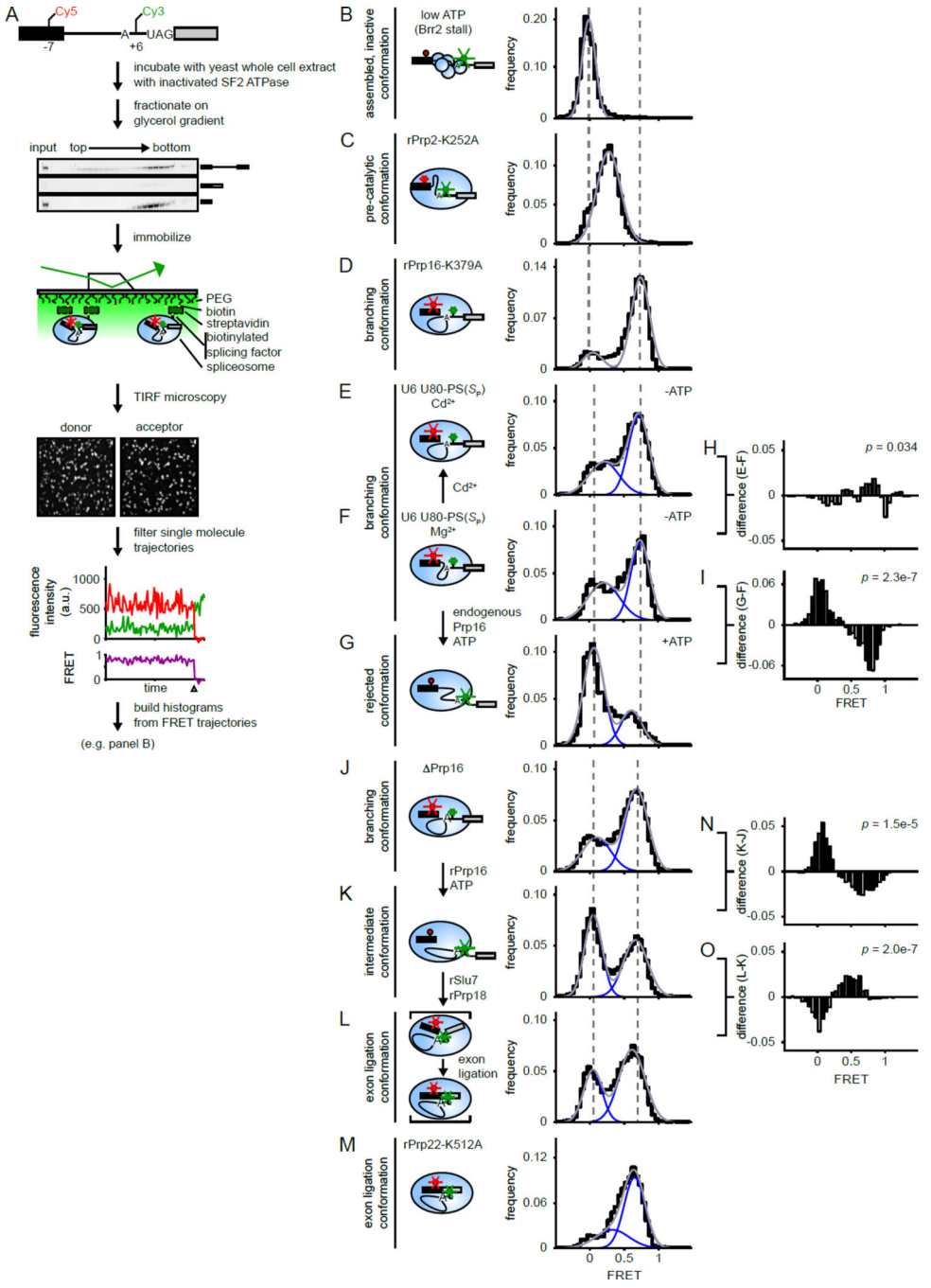

Figure 2. Prp16 Promotes Separation of the 5' Exon and Branch Site During Both Rejection before Branching and Remodeling After Branching

(**A**) Work flow for smFRET experiments. (**B** to **G**, and **J** to **M**) FRET distributions for spliceosomes that were stalled and isolated by gradient fractionation or also chased (E, G, K, and L), as indicated. Histograms (black) were fit with Gaussian peaks (blue) with indicated sum (gray; see Table S2 for details). Diagrams describe substrate connectivity and inferred substrate arrangement based on FRET state for the major spliceosomal conformation in each population. (**H, I, N**, and **O**) Difference histograms conveying changes in FRET distribution

were generated by subtracting the values for each bin in the indicated panels. *p*-values were determined as described in the Supplemental Methods. See also Figure S2 and Table S2.

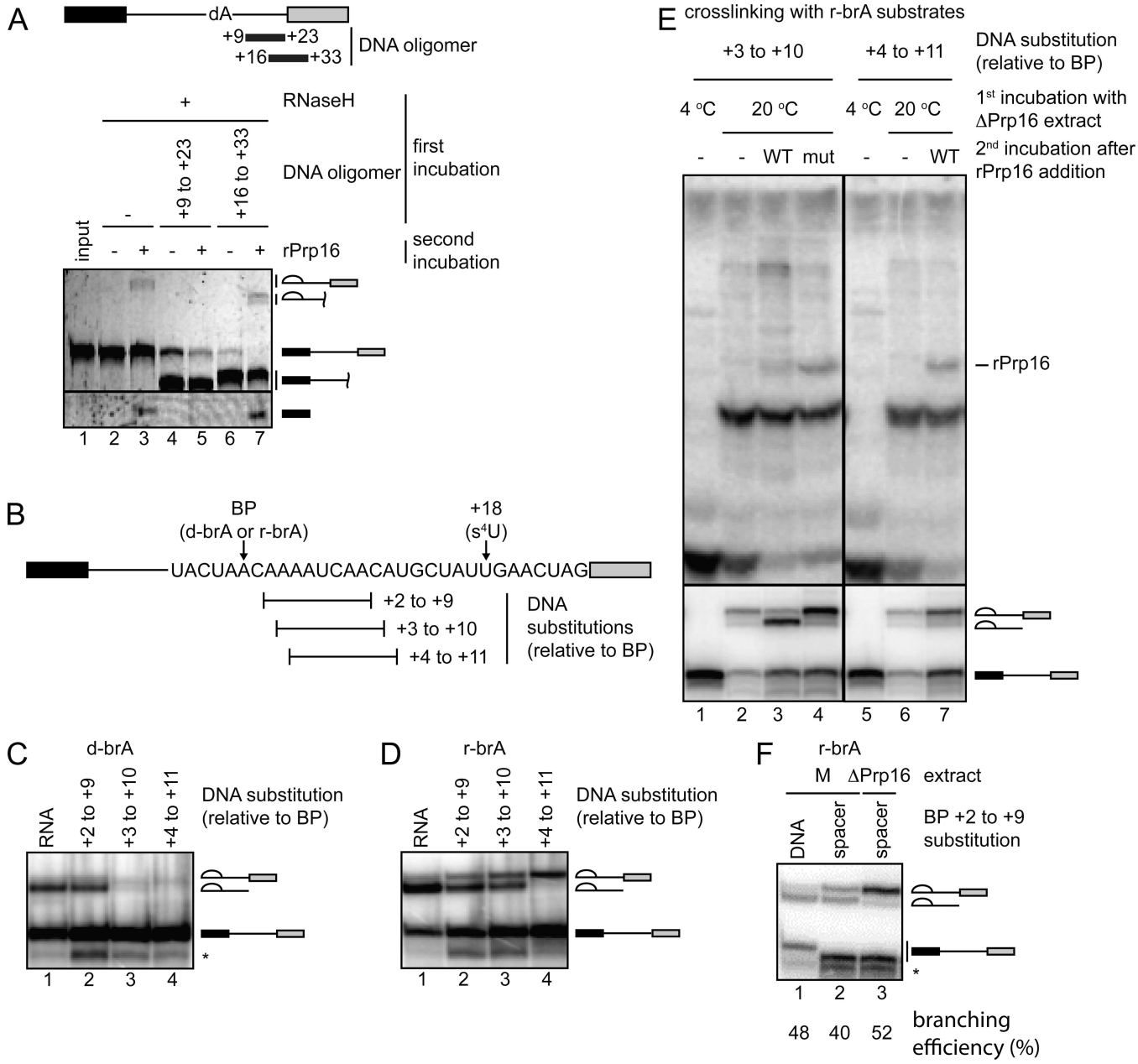

Figure 3. Prp16 Rearranges the Substrate by Translocating Toward, but not Through, Interactions with the Spliceosome

(**A**) The diagram indicates regions of the substrate complementary to DNA oligomers (positions are relative to the branch site) that directed RNaseH cleavage. Pre-mRNA and lariat intermediates were visualized via Cy3. Free 5' exon was visualized via Cy5. (**B**) Schematic of substrates with substitutions downstream of the branch site used in (C to F). (**C, D**, and **F**) Splicing of d-brA (C) or r-brA (D to F) substrates with deoxy (C and D) or carbon spacer (F) substitutions at the positions indicated. Bands marked with an asterisk reflect degradation of the pre-mRNA up to the DNA or spacer substitution. (**E**) The r-brA substrates with the indicated deoxy substitutions and a 4-thio-U modification were incubated and chased as indicated with wild-type (WT) or K379A mutated (mut) rPrp16 and then

crosslinked. Transfer of radiolabel from the substrate to crosslinked protein was analyzed by SDS-PAGE (top panel); splicing was monitored by PAGE (bottom panel). See also Figure S3.

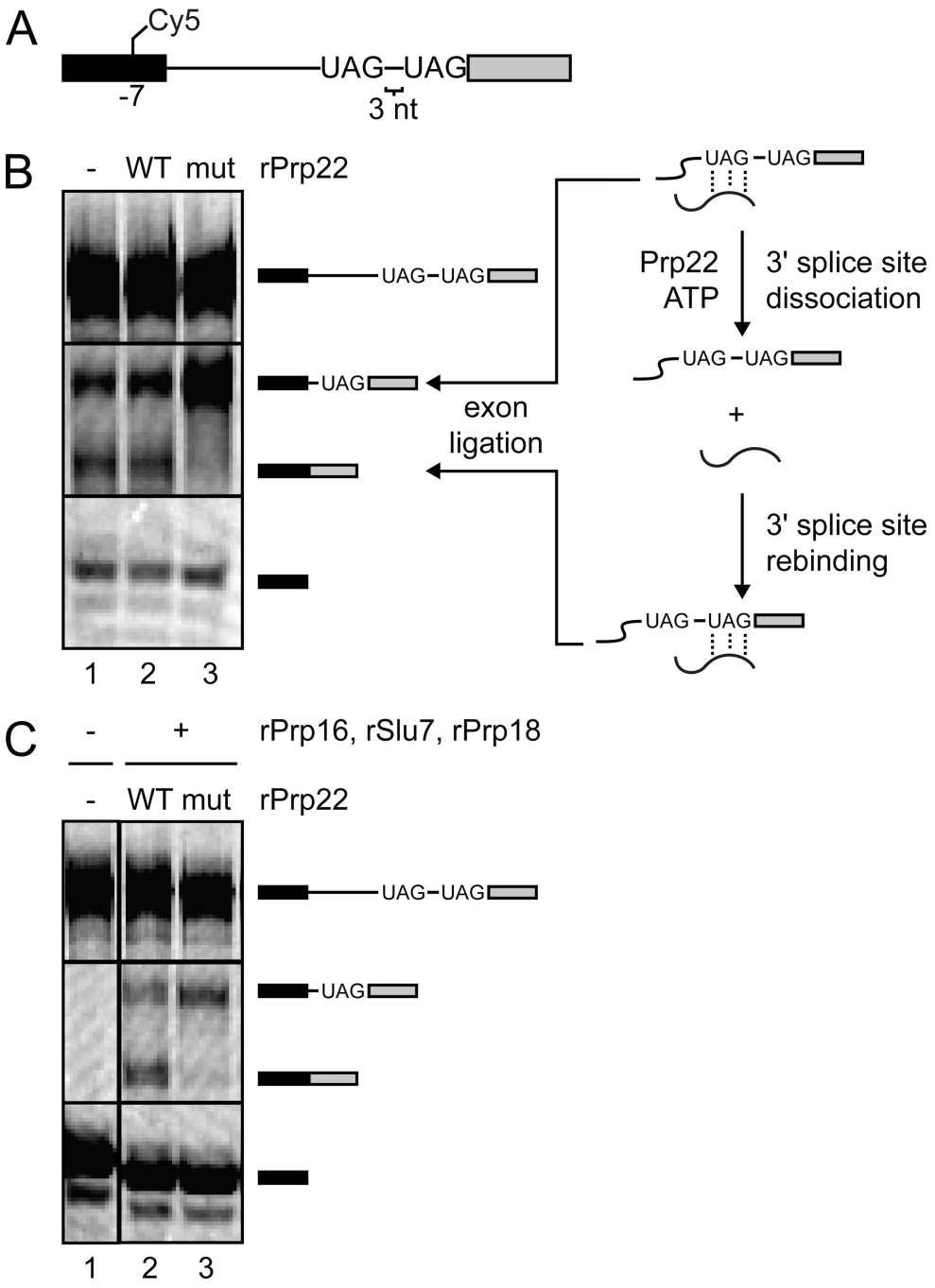

Figure 4. Prp22 Promotes Sampling of Alternative 3' Splice Sites

(**A**) Schematic of synthetic, fluorescently-labeled splicing substrate with tandem 3' splice sites. (**B**) Splicing of the tandem substrate in extract containing only endogenous Prp22 (−) or also exogenous wild-type (WT) or K512A mutated (mut) rPrp22. Splicing was visualized via Cy5. The inferred activity of Prp22 is modeled in the cartoon. (**C**) Isolated, Prp16-depleted spliceosomes assembled on the tandem substrate were incubated with the indicated factors.

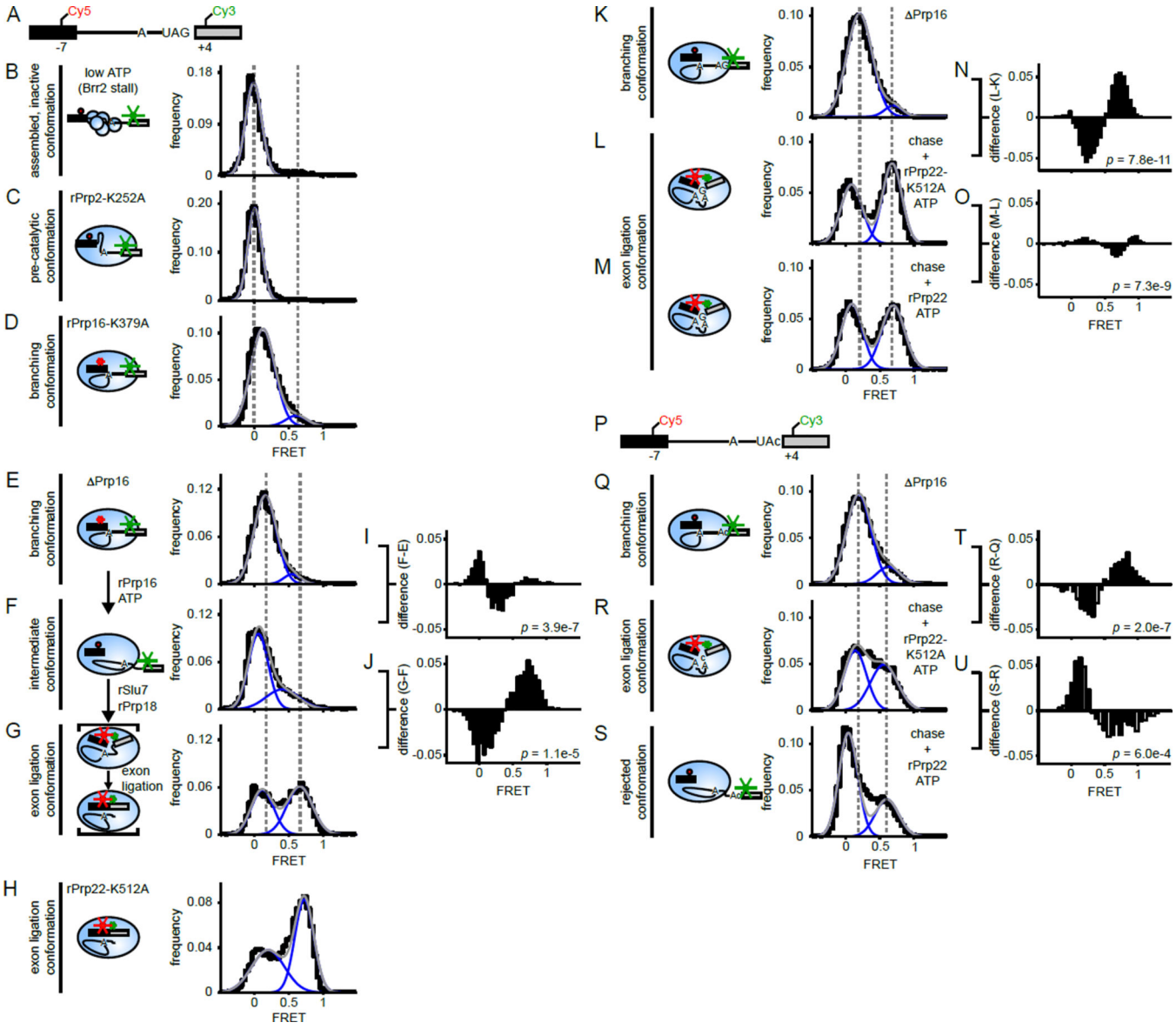

Figure 5. Prp22 Promotes Separation of the 5' Exon and 3' Splice Site During Rejection before Exon ligation

(**A** and **P**) Schematics of fluorescently-labeled synthetic splicing substrates having an optimal (UAG; panel A) or suboptimal (UAc; panel P) 3' splice site. (**B** to **H, K**, to **M**, and **Q** to **S**) FRET distributions for spliceosomes that were stalled and isolated or also chased (F, G, L, M, R, and S) as indicated. For (L, M, R, and S), Prp16-depleted spliceosomes were chased with rPrp16, rSlu7, and rPrp18 (chase) and wild-type or K512A mutated rPrp22, as indicated. Histograms were fit as in Figure 2. (**I, J, N, O, T**, and **U**) Difference histograms and *p*-values were generated as in Figure 2. See also Figure S4 and Table S2.

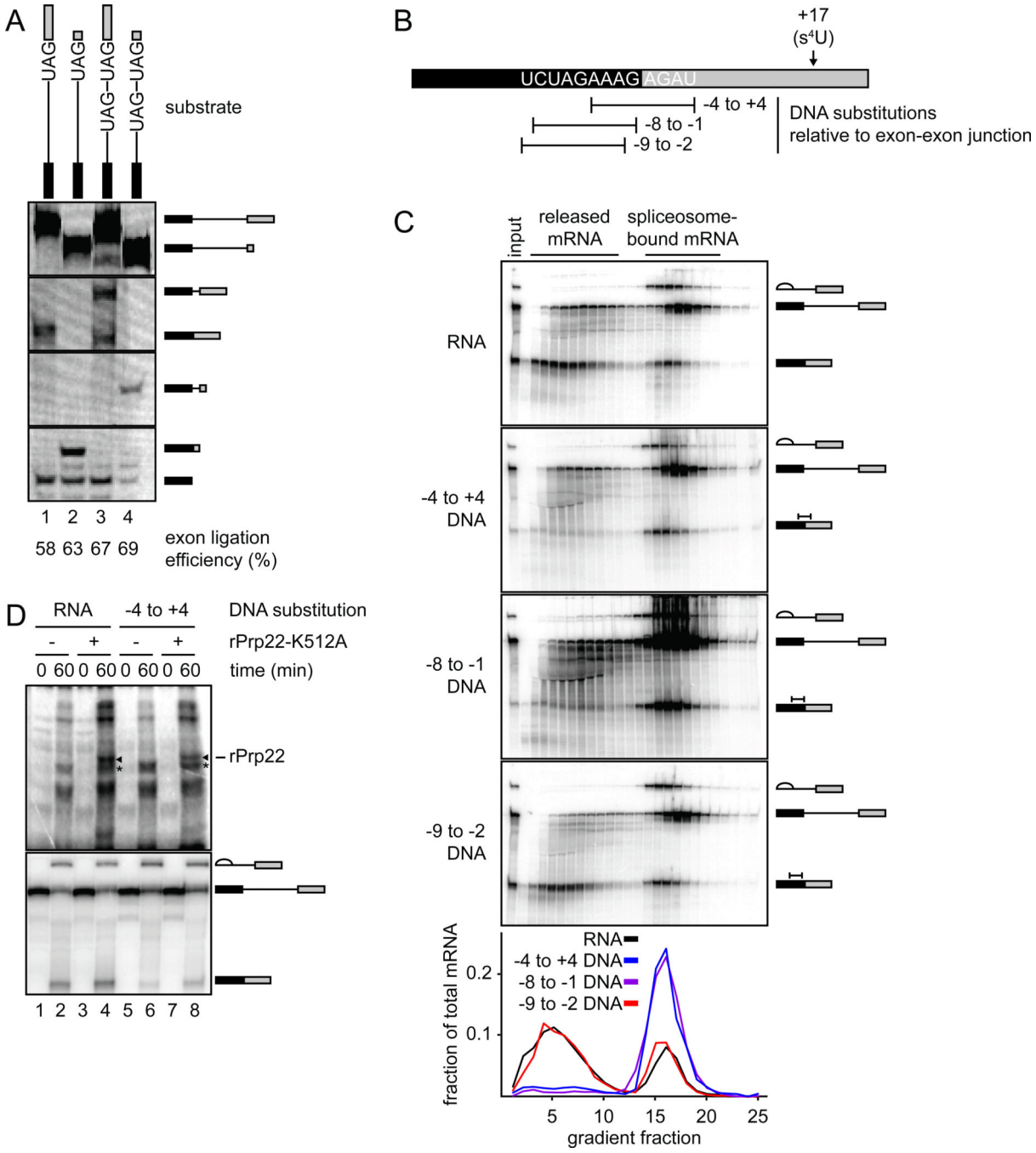

Figure 6. Prp22 Rearranges the Substrate by Translocating Toward, but not Necessarily Through, Interactions with the Spliceosome

(**A**) Splicing of the indicated substrates was visualized via Cy5. The efficiency of branching was 4-fold lower in lane 4, but the efficiency of exon ligation was similar in all four lanes. (**B**) Schematic of substrates with mRNA deoxy substitutions used in (C and D). Positions of the exon-exon junction and s_4U are indicated. (**C**) Substrates with the indicated DNA substitutions were assayed for Prp22-dependent mRNA release. (**D**) Substrates with or without the indicated DNA substitution and with the s_4U modification were incubated as

indicated and then crosslinked. Crosslinking and splicing were monitored as in Figure 3E. Bands marked with an asterisk likely reflect crosslinking by Prp16. See also Figure S5.

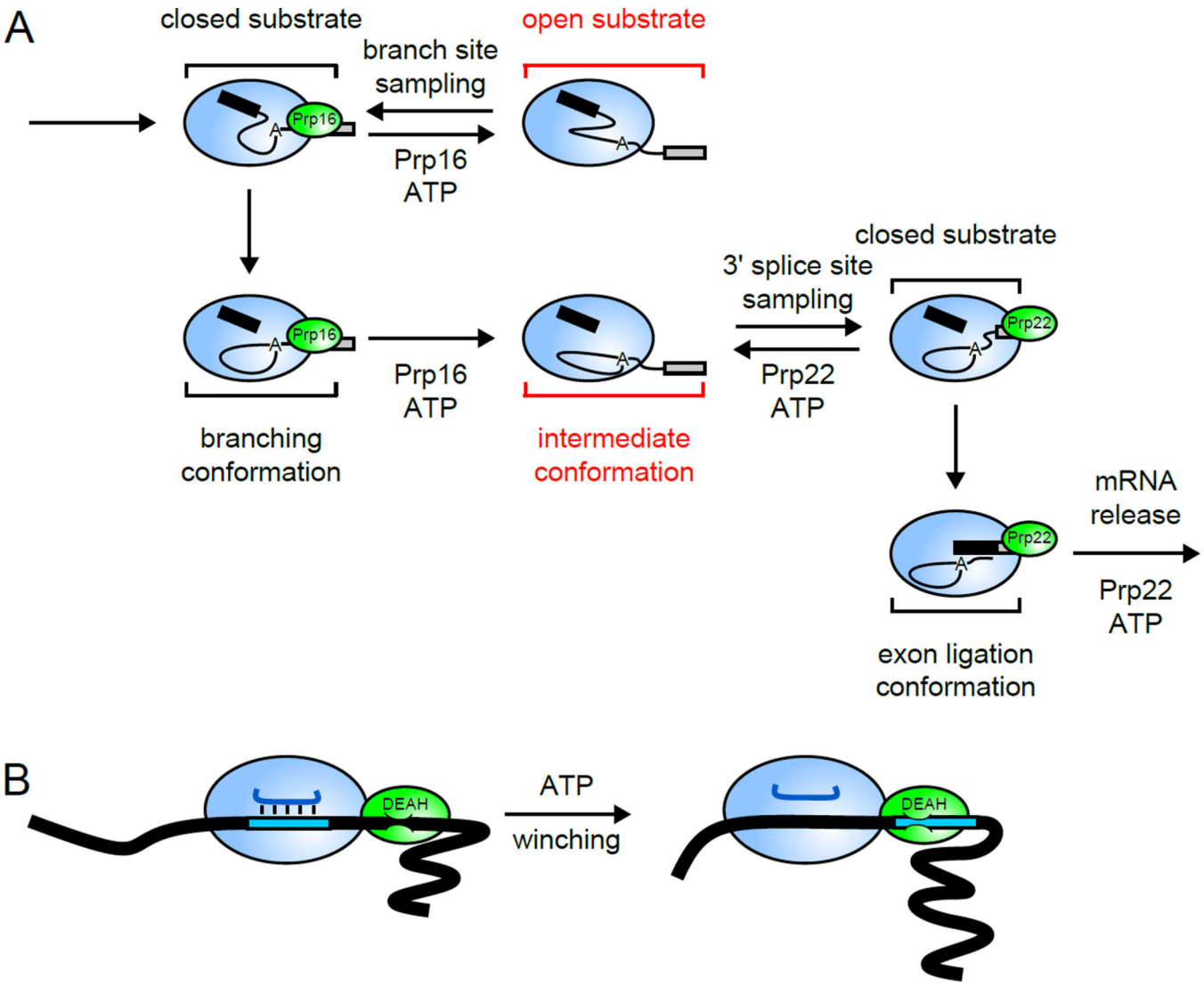

Figure 7. The Function and Mechanism of DEAH-box ATPases at the Catalytic Stage of Splicing

(**A**) Prp16 and Prp22 function as chaperones for splice site selection by separating the splice sites. See text for details. (**B**) A general winching model by which Prp16 and Prp22 promote spliceosomal rearrangements. See text for details. See also Figure S6.